Acoustic radiation force acting on a heavy particle in a standing wave can be dominated by the acoustic microstreaming

Thierry Baasch, Alen Pavlic,* and Jürg Dual
Institute for Mechanical Systems, Swiss Federal Institute of Technology Zurich, 8092 Zurich, Switzerland

We numerically investigate the contribution of the microstreaming to the acoustic radiation force acting on a small elastic spherical particle placed into an ultrasonic standing wave. When an acoustic wave scatters on a particle the acoustic radiation force and the microstreaming appear as nonlinear time-averaged effects. The compressible Navier–Stokes equations are solved up to second order in terms of the small Mach number using a finite element method. We show that when the viscous boundary layer thickness to particle radius ratio is sufficiently large and the particle is sufficiently dense, the acoustic microstreaming dominates the acoustic radiation force. In this case, our theory predicts migration of the particle to the velocity node (pressure antinode).

In 1934, King's desire for a novel method for measuring pressure amplitudes in ultrasonic waves led to the first analytical expression for the acoustic radiation force (ARF) [1], which results from the interaction between background and scattered acoustic fields. Since then, the original assumptions of an incompressible spherical particle in an inviscid fluid have been gradually expanded in complexity due to the increasing interest, mostly in the context of the acoustic manipulation of particles and cells in lab-on-a-chip devices [2–5]. Yosioka and Kawasima in 1955 [6], and Gor'kov in 1962 [7] first supplemented the theory with the contribution of particle's compressibility. More recently, the extension to the viscous fluid was presented by Doinikov in 1994 [8,9], and by Settnes and Bruus in 2012 [10].

When the particle in an inviscid fluid is small compared to the acoustic wavelength of a one-dimensional plane standing wave, its stable position can be determined by the sign of the so-called acoustic contrast factor. King's [1] factor depends on the particle-fluid density ratio, while Yosioka and Kawasima's [6] factor includes also the dependence on the compressibility ratio. Particles of positive acoustic contrast ("heavy") collect at velocity antinodes (pressure nodes), whereas particles of negative contrast ("light") move to velocity nodes (pressure antinodes). This prediction also agrees with experiments, and is commonly applied in particle separation processes [5,11].

Settnes and Bruus [10] modified the acoustic contrast factor to include the viscosity, by considering the fluid to be viscous at the first order in perturbation expansion. They assume the thickness of the viscous boundary layer $\delta = \sqrt{2\eta/(\rho_0\omega)}$ [12], for a medium of dynamic viscosity η, density ρ_0, and angular frequency of ω, to be small with respect to the acoustic wavelength. However, Settnes and Bruus [10] put no restriction on the ratio between δ and particle radius a.

While Settnes and Bruus [10] neglected the viscosity at the second order, Doinikov [8] modeled the fluid as viscous and included the acoustic microstreaming, which is a second-order viscous effect that appears in a form of steady vortices around the particle solely due to the presence of the particle in the acoustic field. In contradiction to the popular first-order viscous model by Settnes and Bruus [10] and inviscid models [1,6,7], Doinikov's [8] model predicts that a heavy particle could be forced towards the velocity node. The discrepancy appears only when the thickness of the viscous boundary layer is larger than the particle radius.

In the last 25 years, this inversion of the direction of the ARF has not been indisputably confirmed or denied, despite experimental efforts by Avetisyan *et al.* [13], and Ran and Saylor [14]; moreover, the sign inversion has been questioned recently by Settnes, Karlsen, and Bruus [10,15]. Here, we provide numerical evidence confirming the sign inversion for a case of a heavy particle in a highly viscous fluid. This phenomenon results due to the viscosity related increase in the contribution of the acoustic microstreaming to the ARF.

In line with previous works [8–10], we neglect thermal effects, and the motion of a viscous fluid is therefore governed by the compressible Navier–Stokes equations and the continuity equation. The pressure p is assumed to be a function of density ρ only. The Navier-Stokes equations are linearized using the perturbation technique. Formally, the physical fields are expanded in a series, $(\cdot) = (\cdot)_0 + (\cdot)_1 + (\cdot)_2 + \cdots$, where $(\cdot)$ represents the field, while the subscript denotes the respective order. We assume that the acoustic velocity amplitude $\|\boldsymbol{v}_1\|$ is small with respect to the speed of sound c_f (small Mach number), i.e., $\|\boldsymbol{v}_1\|/c_f \ll 1$, and that the streaming velocity $\boldsymbol{v}_2$ is small with respect to the acoustic velocity, i.e., $\|\boldsymbol{v}_2\|/\|\boldsymbol{v}_1\| \ll 1$.

Substitution of the perturbed fields into the governing equations, assuming a quiescent fluid at the zeroth order, leads to the set of first-order equations,

$$\rho_0 \frac{\partial \boldsymbol{v}_1}{\partial t} = -\boldsymbol{\nabla} p_1 + \eta \nabla^2 \boldsymbol{v}_1 + \left(\eta_B + \frac{\eta}{3}\right)\boldsymbol{\nabla}(\boldsymbol{\nabla}\cdot\boldsymbol{v}_1), \quad (1)$$

$$\frac{\partial \rho_1}{\partial t} = -\rho_0 \boldsymbol{\nabla}\cdot\boldsymbol{v}_1, \quad (2)$$

$$p_1 = c_f^2 \rho_1, \quad (3)$$

*Corresponding author: apavlic@ethz.ch

with velocity $\boldsymbol{v}$, bulk viscosity η_B, and equilibrium density ρ_0. The first-order fields are assumed to be harmonic with factor $e^{i\omega t}$. The solid particle is modeled using the equations of linear elasticity [16], with the primary and the secondary speed of sound, c_P and c_S, respectively. The acoustic fields, comprising velocity $\boldsymbol{v}_1$ and pressure p_1, are assumed to be sums of background fields (bg) and scattered fields (sc), namely, $(\cdot)_1 = (\cdot)_1^{\text{bg}} + (\cdot)_1^{\text{sc}}$. We assume a one-dimensional plane standing wave along the z direction of the cylindrical coordinate system. The background velocity field is set to

$$\boldsymbol{v}_1^{\text{bg}} = \text{Re}\left[\frac{\varphi_a}{2}ik(e^{ikz} - e^{-ikz})e^{i\omega t}\right]\boldsymbol{e}_z, \quad (4)$$

with the corresponding velocity potential amplitude

$$\varphi_a = -\frac{p_a}{i\omega\rho_0 + (\eta_B + \frac{4}{3}\eta)k^2}, \quad (5)$$

with pressure amplitude p_a, and wave number for viscous fluids k [17]. The acoustic wavelength can then be defined through the wave number as $\lambda = 2\pi/\text{Re}[k]$. At the fluid-solid interface, we impose the continuity of velocity and stress. The fluid is assumed to be unbounded, and the first-order fields therefore converge to the background fields with the increasing distance from the particle.

Applying the perturbation theory up to second order and taking the time average $\langle(\cdot)\rangle := \frac{1}{T}\int_T(\cdot)dt$ over an oscillation period T yields the equations of acoustic streaming [8,10],

$$\nabla\langle p_2\rangle - \eta\nabla^2\langle\boldsymbol{v}_2\rangle - \left(\eta_B + \frac{\eta}{3}\right)\nabla(\nabla\cdot\langle\boldsymbol{v}_2\rangle) = -\rho_0\nabla\cdot\langle\boldsymbol{v}_1\boldsymbol{v}_1\rangle, \quad (6)$$

$$\rho_0\nabla\cdot\langle\boldsymbol{v}_2\rangle + \nabla\cdot\langle\rho_1\boldsymbol{v}_1\rangle = 0. \quad (7)$$

At the second order, we impose the no-slip boundary condition on a fluid at the fluid-solid interface, namely,

$$\langle\boldsymbol{v}_2\rangle = -\left\langle\left(\int\boldsymbol{v}_1 dt\cdot\nabla\right)\boldsymbol{v}_1\right\rangle \quad \text{at the interface}, \quad (8)$$

where the right-hand-side term is the negative Stokes' drift [18–20] that compensates for the first-order oscillations of the interface. The contribution of the streaming due to the attenuation of the background field, which is present even in the absence of the particle, was neglected by Doinikov [8,9]. In our simulations we also found this contribution to be negligible. In experiments, however, the presence of boundaries could lead to more significant Rayleigh streaming [12], which leads to an additional drag force on the particle. However, it has been shown [21] that the streaming at the center of a wide channel can be very low and thus small compared to the microstreaming that originates from the presence of the particle.

We consider the time-averaged ARF on the particle to be the net mean force,

$$\boldsymbol{F}_{\text{rad}} := \left\langle\int_{S(t)}\boldsymbol{\sigma}\cdot\boldsymbol{n}(t)dS\right\rangle, \quad (9)$$

integrated over the oscillating particle surface $S(t)$, with outward pointing surface normal $\boldsymbol{n}(t)$, and stress tensor $\boldsymbol{\sigma}$.
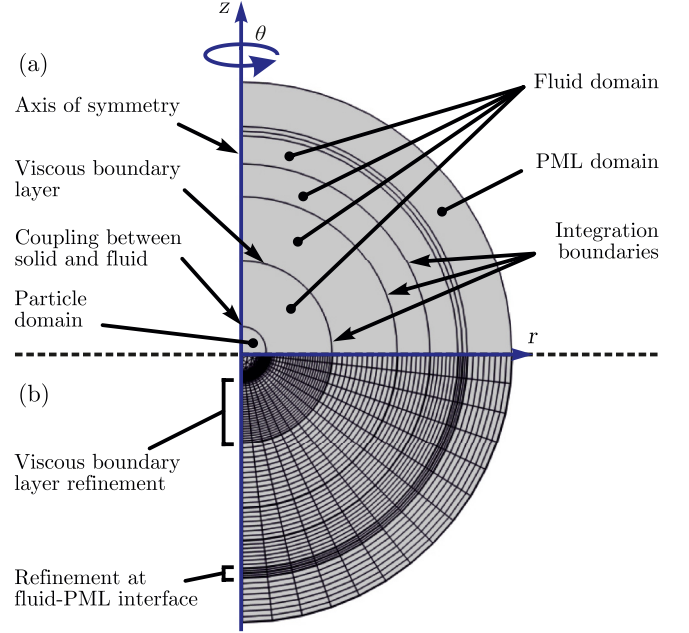
FIG. 1. The first-order COMSOL model; (a) the geometry and (b) the mesh of the model, which is symmetric with respect to the z axis of the cylindrical coordinate system (r, θ, z).

Doinikov [8] demonstrated that the expression for the ARF, accurate to the second order, can be written as

$$\boldsymbol{F}_{\text{rad}} = \int_{S_0}\left[\langle\boldsymbol{\sigma}_2\rangle - \rho_0\langle\boldsymbol{v}_1\boldsymbol{v}_1\rangle\right]\cdot\boldsymbol{n}_0 dS, \quad (10)$$

where the difference between the mean second-order stress tensor and Reynolds stress [22] is mapped onto the normal $\boldsymbol{n}_0$ pointing out of the arbitrary static surface S_0 enclosing the particle, and integrated over S_0. The viscous effects at the second order, including microstreaming, are contained in the stress tensor $\langle\boldsymbol{\sigma}_2\rangle$. The first- and the second-order viscous equations are solved consecutively using two finite element method (FEM) models (COMSOL Multiphysics 5.4 framework [23]). The geometry and the mesh used for the first-order FEM model are shown in Fig. 1. We use a perfectly matched layer (PML) that absorbs outgoing waves to model the fluid domain as being infinite. For the second-order model, we use the same geometry and mesh as depicted in Fig. 1, but without PML and particle domains. The infinite fluid domain assumption is satisfied by using the domain large enough to mitigate the effect of boundaries on the computed ARF.

The mesh is refined at the fluid-PML interface to minimize the reflections back into the fluid domain and in the region of the viscous boundary layer to improve the discretization of high-velocity gradients. Integration boundaries placed at various distances from the particle are used for the validation of the model, and for the computation of the ARF. Since the problem is symmetric with respect to the direction of the wave propagation, we define the only nonzero component of the ARF as $F_{\text{rad}} = \boldsymbol{F}_{\text{rad}}\cdot\boldsymbol{e}_z$, with unit vector $\boldsymbol{e}_z$ directed along the axis of symmetry.

Convergence studies were performed to determine the required amount of mesh elements and the minimal fluid domain
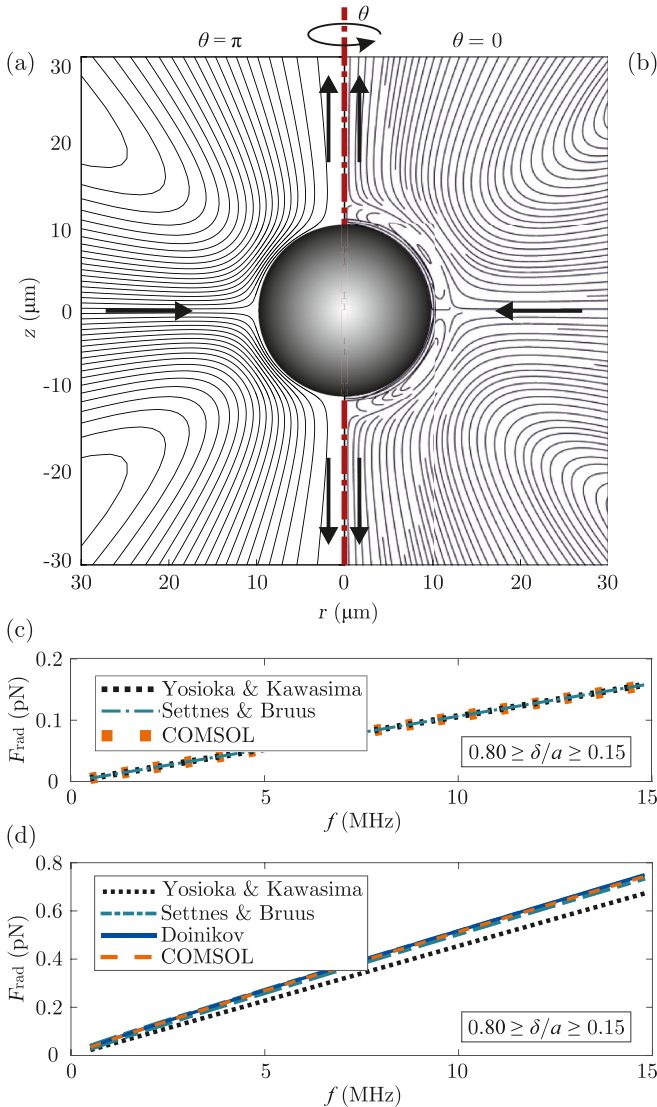
FIG. 2. (a) Comparison of Eulerian streaming patterns around a rigid sphere by Rednikov and Sadhal [25], and (b) by our numerical model. The particle of 10 μm radius is positioned at a velocity antinode of a standing wave with frequency of 0.6 MHz, in water. The flow direction is indicated by arrows. (c) The ARF on a polystyrene sphere, and (d) on a copper sphere in water, with respect to the frequency f. The particle of 1 μm radius is positioned between the velocity node and the antinode.

TABLE I. The material parameters for water (H_2O) [27,28], oil [15], polystyrene (PS) [29], and copper (Cu) [29]. The viscous acoustic contrast factor (Φ_{vis}) is computed using Eq. (50b) from [10]; the inviscid contrast factor (Φ_{inv}) results from the same expression, but assuming $\delta = 0$, which recovers the expression from the inviscid theory [6].

	PS/H$_2$O	Cu/H$_2$O	Cu/oil	Unit
ρ_0	998.2	998.2	922.6	kg m^{-3}
ρ_p	1050	8930	8930	kg m^{-3}
c_f	1482	1482	1445	m s^{-1}
c_P	2400	5010	5010	m s^{-1}
c_S	1150	2270	2270	m s^{-1}
η	1.002	1.002	41.5	mPa s
η_B	3.09	3.09	89.3	mPa s
Φ_{inv}	0.18	0.75	0.76	mPa s
Φ_{vis} at 0.5 MHz	0.18	1.1	2.1	
Φ_{vis} at 15 MHz	0.18	0.82	1.19	
p_a	100	100	100	kPa

size. For simulations, we chose the fluid thickness of $100 \times a$, in order to eliminate the influence of the outer fluid boundary (details in the Supplemental Material [24]).

We compare the streaming pattern obtained by our model [Fig. 2(b)] to the analytical solution for a rigid sphere by Rednikov and Sadhal [25] [Fig. 2(a)]. A rigid particle ($a = 10$ μm) in water is positioned at the velocity antinode of a standing wave with $f = 0.6$ MHz. The outer streaming patterns agree and show the fluid flowing away from the sphere along the z axis. The numerical simulation reveals inner vortices contained near the viscous boundary layer, which are driving the outer streaming, and which do not appear in the analytical solution since they used the limiting velocity approach [26].

To further validate our model, the ARF is analyzed for a polystyrene [Fig. 2(c)] and copper [Fig. 2(d)] particle immersed in water and positioned between the velocity node and the antinode. The frequency range of 0.5 MHz $\leqslant f \leqslant 15$ MHz, considering water, yields a minimum acoustic wavelength λ of 99 μm and a maximum thickness of the viscous boundary layer δ of 0.80 μm. Therefore, the wavelength is large and the viscous boundary layer is small relative to the particle radius of 1 μm. In this regime the models by Settnes and Bruus [10], Doinikov [8], and our numerical model mutually agree. The agreement of our numerical model, denoted by "COMSOL," with the theory by Settnes and Bruus [10] is demonstrated using a polystyrene particle in Fig. 2(c). In that case the model by Doinikov [8] is not applicable due to its rigid sphere assumption. However, Doinikov's model [8] agrees well with the numerical model and the model by Settnes and Bruus [10] for a less compressible copper particle, as shown in Fig. 2(d). The model by Yosioka and Kawasima [6] agrees with the numerical model for polystyrene, but shows a deviation of up to 50% for copper at 0.5 MHz. The deviation, which is mostly due to the effect of viscosity at the first order, decreases to about 10% at 15 MHz. The effect of viscosity at the first order can be estimated by comparing the inviscid [6] (Φ_{inv}) and the first-order viscous [10] (Φ_{vis}) acoustic contrast factors. The difference between Φ_{inv} and Φ_{vis} is significant for a copper particle in water and goes from 0.3565 at 0.5 MHz to 0.0748 at 15 MHz, but negligible for a polystyrene particle, where it goes from 0.0003 at 0.5 MHz to 0.0001 at 15 MHz. The factors are listed in Table I, along with the other material parameters that are used in simulations.

In addition to the difference in the compressibility assumption, the theoretical models treat the viscosity of the surrounding fluid differently. Doinikov [8] considers the viscosity at the first and second order and thus includes the contribution of the microstreaming around the particle. Settnes and Bruus [10] neglect microstreaming by assuming the fluid to be inviscid at the second order. Both models are derived for the limits

(a)

(b)
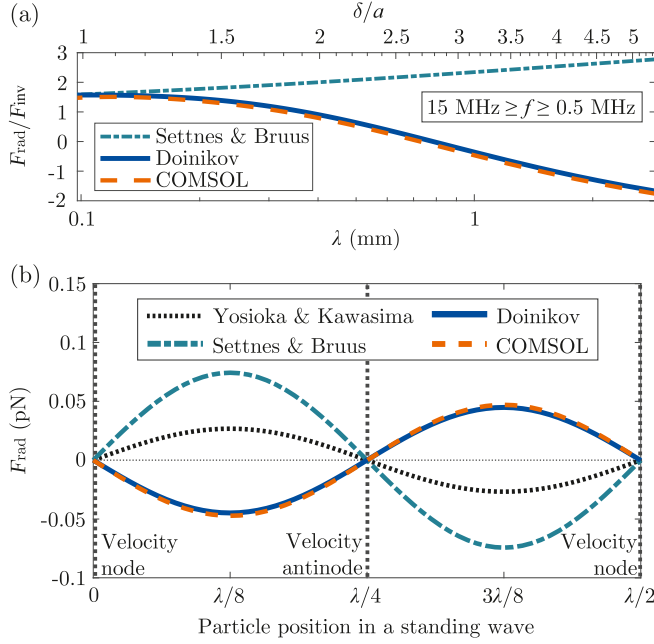
FIG. 3. The ARF on a copper sphere ($a = 1$ μm) in oil. (a) The force with respect to the relative thickness of the viscous boundary layer. The forces are normalized with respect to the force F_{inv} from the inviscid model [6]. The particle is positioned between the velocity node and the antinode. The boundary layer thickness changes due to the frequency sweep, indicated by the acoustic wavelength λ. (b) The ARF for different theories and our numerical model COMSOL. The force is analyzed with respect to the particle position in a standing wave with a frequency of 0.5 MHz. Our model agrees with the model by Doinikov [8] and predicts a different sign of the ARF compared to the models by Settnes and Bruus [10] and Yosioka and Kawasima [6].

of $a \ll \lambda$ and $\delta \ll \lambda$, and with no restriction on the relative viscous boundary layer thickness δ/a. These two theories disagree for a copper particle with radius of 1 μm immersed in oil at $\delta/a > 1$. In Fig. 3(a), we normalized the force by the force from the inviscid model [6] to show the counteracting effects of the viscosity at the first and second order. Doinikov's model predicts a decrease of the normalized ARF with the increase of δ/a, whereas the model by Settnes and Bruus [10] predicts an increase of the normalized ARF. Our numerical model agrees with the model by Doinikov [8] throughout the whole range of δ/a, experiencing the change in the direction of the force at $\delta/a = 2.75$. This leads to the particle being forced towards the velocity node. In Fig. 3(b), the ARF is analyzed for the same case, at $f = 0.5$ MHz, as a function of the particle position in a standing wave. The position of the center of the particle is varied between two velocity nodes (at $z = 0$ and $z = \lambda/2$). Our numerical results support the second-order viscous theory by Doinikov [8], predicting the force of opposite direction compared to the first-order viscous theory by Settnes and Bruus [10].

For a further analysis, we expand the expression from Eq. (10) by applying the Newton's viscosity law, and divide it into a sum of three force contributions, namely, $F_{rad} =$

(a)

(b)
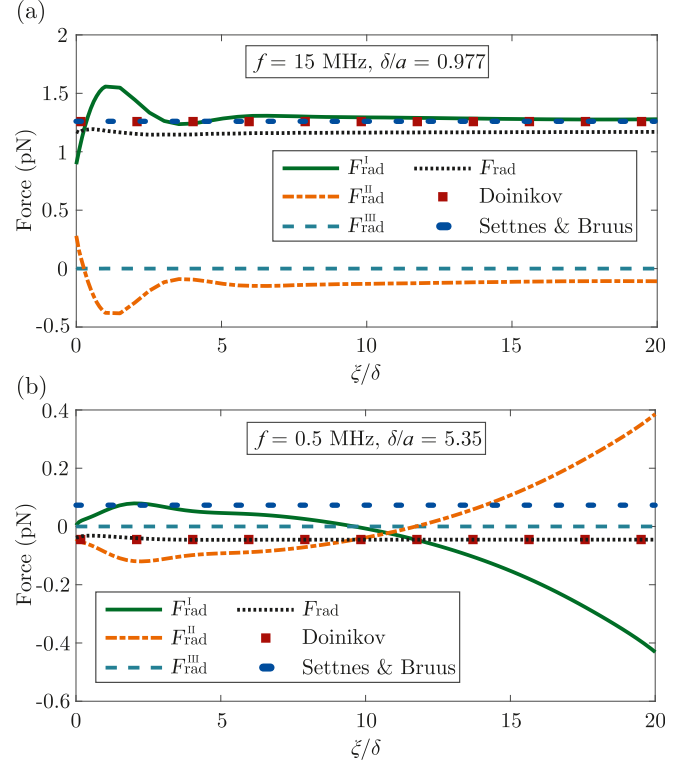
FIG. 4. The individual force contributions to the ARF, according to Eqs. (11)–(13), for a copper sphere in oil, positioned between the velocity node and the antinode. The forces are plotted with respect to the distance of the integration surface from the particle surface, i.e., $\xi = r - a$, normalized with the thickness of the viscous boundary layer δ. Here, the thickness of the fluid domain was increased to $140 \times a$. The ARF according to Doinikov [8] and Settnes and Bruus [10] is included for a reference.

$F_{rad}^{I} + F_{rad}^{II} + F_{rad}^{III}$, with

$$F_{rad}^{I} = \boldsymbol{e}_z \cdot \int_{S_0} \left[- \langle p_2 \rangle \mathbf{I} - \rho_0 \langle \boldsymbol{v}_1 \boldsymbol{v}_1 \rangle \right] \cdot \boldsymbol{n}_0 \, dS, \quad (11)$$

$$F_{rad}^{II} = \boldsymbol{e}_z \cdot \int_{S_0} \eta \big(\langle \boldsymbol{\nabla} \boldsymbol{v}_2 \rangle + \langle \boldsymbol{\nabla} \boldsymbol{v}_2 \rangle^\top \big) \cdot \boldsymbol{n}_0 \, dS, \quad (12)$$

$$F_{rad}^{III} = \boldsymbol{e}_z \cdot \int_{S_0} \left(\eta_{\mathrm{B}} - \frac{2}{3}\eta \right) \langle \boldsymbol{\nabla} \cdot \boldsymbol{v}_2 \rangle \boldsymbol{n}_0 \, dS. \quad (13)$$

In Fig. 4, we show the values of separate contributions for a copper particle in oil, at frequencies of (a) 15 MHz and (b) 0.5 MHz. The distance ξ, between the spherical integration surface and particle surface (at $\xi = 0$), is increased in terms of the thickness of the viscous boundary layer. We observe that the contribution of the gradient of the streaming velocity (F_{rad}^{II}) grows to the same order as the pressure contribution (F_{rad}^{I}) when increasing δ/a from 0.977 in Fig. 4(a) to 5.35 in Fig. 4(b). The contribution of the divergence of the streaming velocity to the ARF (F_{rad}^{III}) is negligible at both ends of the frequency range. This validates the common assumption that the time-averaged second-order flow, i.e., the streaming flow, is incompressible [8,9]. In addition, the total force (F_{rad}) is,

as expected from the theory [8], constant irrespective of the integration surface.

We have established that in a standing wave in highly viscous fluids ($\delta/a > 1$), the ARF can force particles that are less compressible and of higher density than the surrounding fluid towards the velocity node (pressure antinode). This phenomenon is due to the dominant contribution of the second-order viscous effect called the acoustic microstreaming. The demonstrated behavior contradicts the inviscid theories [1,6,7], and confirms the second-order viscous theory by Doinikov from 1994 [8], who considered the acoustic microstreaming. Our numerical model shows that the contribution of microstreaming to the ARF should not be neglected when the relative thickness of the viscous boundary layer is high ($\delta/a > 1$). The first-order viscous models that neglect the viscosity at the second order, such as the model by Settnes and Bruus [10], are consequently valid only in a limited range in terms of δ/a. When the viscosity of the medium is relatively low ($\delta/a < 1$), our model and models by Doinikov [8] and Settnes and Bruus [10] coincide. To observe the suggested effects in experiments, an acoustic device with a wide channel could be used to minimize the Rayleigh streaming. The effect is strongest for heavy particles in highly viscous fluids; for example, copper particles in oil.

T.B. and A.P. contributed equally to this work.

---

[1] L. V. King, Proc. R. Soc. London, Ser. A **147**, 212 (1934).

[2] W. T. Coakley, Trends Biotechnol. **15**, 506 (1997).

[3] M. Gröschl, Acta Acust. Acust. **84**, 432 (1998).

[4] F. Petersson, A. Nilsson, C. Holm, H. Jönsson, and T. Laurell, Analyst **129**, 938 (2004).

[5] T. Laurell, F. Petersson, and A. Nilsson, Chem. Soc. Rev. **36**, 492 (2007).

[6] K. Yosioka and Y. Kawasima, Acta Acust. Acust. **5**, 167 (1955).

[7] L. P. Gor'kov, Sov. Phys. Dokl. **6**, 773 (1962).

[8] A. A. Doinikov, Proc. R. Soc. London, Ser. A **447**, 447 (1994).

[9] A. A. Doinikov, J. Fluid Mech. **267**, 1 (1994).

[10] M. Settnes and H. Bruus, Phys. Rev. E **85**, 016327 (2012).

[11] A. Lenshof, C. Magnusson, and T. Laurell, Lab Chip **12**, 1210 (2012).

[12] L. Rayleigh, Philos. Trans. R. Soc. London **175**, 1 (1884).

[13] A. G. Avetisyan, V. S. Arakelyan, O. V. Bagdasaryan, and A. K. Dudoyan, Sov. Phys. Acoust. **31**, 227 (1985).

[14] W. Ran and J. Saylor, J. Acoust. Soc. Am. **137**, 3288 (2015).

[15] J. T. Karlsen and H. Bruus, Phys. Rev. E **92**, 043010 (2015).

[16] K. F. Graff, *Wave Motion in Elastic Solids* (Dover, New York, 2012).

[17] D. T. Blackstock, *Fundamentals of Physical Acoustics* (ASA, New York, 2001).

[18] D. G. Andrews and M. E. McIntyre, J. Fluid Mech. **89**, 609 (1978).

[19] O. Bühler, *Waves and Mean Flows* (Cambridge University Press, Cambridge, UK, 2014).

[20] M. S. Longuet–Higgins, Proc. R. Soc. London, Ser. A **454**, 725 (1998).

[21] P. B. Muller, M. Rossi, A. G. Marin, R. Barnkob, P. Augustsson, T. Laurell, C. J. Kähler, and H. Bruus, Phys. Rev. E **88**, 023006 (2013).

[22] J. Lighthill, J. Sound Vib. **61**, 391 (1978).

[23] Comsol Multiphysics 5.4, www.comsol.com, 2018.

[24] See Supplemental Material at http://link.aps.org/supplemental/10.1103/PhysRevE.100.061102 for convergence studies.

[25] A. Y. Rednikov and S. S. Sadhal, J. Fluid Mech. **667**, 426 (2011).

[26] W. L. Nyborg, J. Acoust. Soc. Am. **30**, 329 (1958).

[27] J. Rumble, *CRC Handbook of Chemistry and Physics* (CRC Press, Boca Raton, FL, 2018).

[28] M. J. Holmes, N. G. Parker, and M. J. W. Povey, J. Phys.: Conf. Ser. **269**, 012011 (2011).

[29] A. R. Selfridge, IEEE Trans. Sonics Ultrason. **32**, 381 (1985).